J Appl Electrochem (2008) 38:695–701
DOI 10.1007/s10800-008-9490-x

ORIGINAL PAPER

Activity of a novel titanium-supported bimetallic PtSn/Ti electrode for electrocatalytic oxidation of formic acid and methanol

Qingfeng Yi · Jingjing Zhang · Aicheng Chen · Xiaoping Liu · Guorong Xu · Zhihua Zhou

Received: 5 September 2007 / Revised: 24 December 2007 / Accepted: 18 January 2008 / Published online: 5 February 2008

Abstract Bimetallic platinum–tin nanoparticles were co-deposited on a titanium surface using a simple one step hydrothermal method process. The electrochemical catalytic activity of this titanium-supported nanoPtSn/Ti electrode towards the oxidation of formic acid and methanol in 0.5 M H_2SO_4 was evaluated by voltammetric techniques, chronoamperometric responses and electrochemical impedance spectra (EIS). According to the cyclic voltammograms of the oxidation of both formic acid and methanol, the nanoPtSn/Ti presents high anodic current densities and low onset potentials. Potential-time transient measurements show that the nanoPtSn/Ti exhibits high steady-state current densities for the oxidation of both formic acid and methanol. The EIS data indicate that the nanoPtSn/Ti presents very low electrochemical impedance values, showing that for the oxidation of both formic acid and methanol, low charge transfer resistances are present on the nanoPtSn/Ti catalyst. This confirms the high electrocatalytic activity of the nanoPtSn/Ti for the formic acid and methanol oxidation.

Keywords Bimetallic PtSn · Formic acid oxidation · Methanol oxidation · Titanium substrate

Q. Yi (✉) · X. Liu · G. Xu · Z. Zhou
School of Chemistry and Chemical Engineering, Hunan University of Science and Technology, Xiangtan 411201, China
e-mail: yqfyy2001@yahoo.com.cn

J. Zhang
Chemistry Science and Technology School, Zhanjiang Normal University, Zhanjiang 524048, China

A. Chen
Department of Chemistry, Lakehead University, Thunder Bay, ON, Canada P7B 5E1

1 Introduction

Methanol and formic acid are promising liquid fuels for micro fuel cells [1]. Direct methanol (formic acid) fuel cells (DMFCs or MFAFCs) have been receiving considerable attention because of their potential applications as clean and portable power units for small generating plants and power cars [2–6]. One of the key problems in DMFCs or MFAFCs is the development of anodic materials with high electroactivity towards the oxidation of methanol and formic acid. It is well known that platinum is an effective electrocatalyst for these oxidations [7, 8]. In order to enhance the electroactivity of pure platinum, bimetallic or ternary metal electrocatalysts containing Pt have been fabricated. Bimetallic PtRu electrocatalysts have been intensively investigated and show high activity for methanol oxidation [9–18]. Electrochemical oxidation of both methanol and formic acid on bimetallic PtIr catalysts has been carried out [9, 19]. Electrocatalytic activity of platinum alloys with the first row transition metals towards methanol oxidation has been reviewed by Antolini et al. [7]. In addition, Shijun Liao and co-workers prepared the ternary PtRuIr catalysts supported on nanotubes and evaluated their electroactivity for methanol oxidation [20]. With respect to formic acid oxidation, its effective catalytic materials include pure Pd [1], carbon-supported Pd nanoparticles [21], bimetallic PtPd [22], and PtIr [19]. However, the high cost of such metals as platinum, ruthenium, iridium and palladium, limits their practical application. It is required to develop more efficient Pt catalysts having reasonable or economical costs. One approach to achieve this is to use platinum alloys to replace pure Pt. Among these alloys bimetallic PtSn catalysts have been demonstrated to exhibit attractive electroactivity towards methanol oxidation [9]. Stalnionis et al. have reported the

modification of a Pt surface by spontaneous Sn deposition through a simple "dip-coating" method under open-circuit conditions and studied its electroactivity for oxidation of CO, formaldehyde, formic acid, and methanol [23]. Golikand et al. prepared a Pb electrode modified by PtSn microparticles by electrochemical deposition of bimetallic PtSn particles from an aqueous sulfuric acid solution containing H_2PtCl_6 and $SnCl_4 \cdot 5H_2O$ on the surface of Pb [24]. Results showed that the catalytic activity of Pt particles is further enhanced when Sn is co-deposited in Pt particles. Leger fabricated a carbon supported PtSn catalyst by the co-reduction of platinum and tin from the two different metallic salts and studied its electrocatalytic activity towards ethanol oxidation [25]. Similarly, a carbon supported PtSn alloy for ethanol oxidation was prepared by Jiang et al. using a modified polyol method [26]. Guo and co-workers prepared a Sn/Pt bimetallic nanotube array in the pores of a porous anodic aluminum oxide template and investigated its electrocatalytic activity for methanol oxidation [27]. In addition, Liu et al. reported the microwave heated polyol synthesis of carbon-supported PtSn nanoparticles for methanol electrooxidation [28]. The development of electrocatalysts having reasonable costs and high electroactivity for the oxidation of formic acid and methanol is of considerable interest to fuel cells.

In this paper, we report the successful preparation of a novel titanium-supported nano-scale bimetallic PtSn electrode (nanoPtSn/Ti) using a simple hydrothermal treatment method consisting of a one step process. Electrochemical activity of the nanoPtSn/Ti towards the oxidation of formic acid and methanol was assessed by voltammetric techniques, chronoamperometric measurements and electrochemical impedance spectra (EIS).

2 Experimental

2.1 Preparation of nanoPtSn/Ti

Before deposition of platinum and tin on the surface of titanium substrate, the pieces of titanium foil were subjected to careful pretreatment: first, they were washed with Nanopure water (18.2 MΩ cm), then etched in an 18% HCl solution at 85 °C for 10 min to remove the oxide layer on the titanium surface; after the etched Ti pieces were washed with Nanopure water, they were finally further cleaned in a ultrasonic generator for 5 min. The treated substrate pieces were placed on the bottom of a Teflon Holder lined autoclave containing 0.5 mL formaldehyde (5%), 10 mL $H_2PtCl_6 \cdot 6H_2O$ (0.8 g L^{-1}) and 1.0 mL $SnCl_2$ (0.42 g $SnCl_2 \cdot 2H_2O$ in 60 mL isopropanol), and then heated at 180 °C for 10 h. After cooling to room temperature, the coated substrates were removed from the Holder, air dried, then rinsed with Nanopure water. This process resulted in the fabrication of the nanoPtSn/Ti electrode. The geometric surface area of the nanoPtSn/Ti electrode is 0.20 cm^2 which was used as the calculation of current density.

The texture of the sample was characterized using scanning electron microscopy (SEM) taken on a JEOL 5900LV. X-ray diffractogram of the catalyst was obtained in D/MAX2500X Diffractometer (Japan), operating with Cu $K\alpha$ radiation generated at 40 kV and 250 mA.

2.2 Chemicals and electrochemical measurements

All chemicals used in this work were reagent grade products and were used without further purification. Aqueous solutions were prepared with Nanopure water (18.2 MΩ cm). $H_2PtCl_6 \cdot 6H_2O$, $SnCl_2 \cdot 2H_2O$, H_2SO_4, HCOOH, and CH_3OH were purchased from Aldrich.

The electrochemical experiments were conducted using a VoltaLab 40 Potentiostat PGZ301. A conventional three-electrode cell was used with a saturated calomel electrode (SCE:Hg/Hg_2Cl_2/sat. KCl) as reference and a large platinum wire as counter electrode. All potentials reported in this paper are referred to the SCE which was positioned as close to the working electrode as possible by means of a Luggin capillary. Electrochemical methods used in this work included cyclic voltammograms, linear sweep voltammetry, chrono amperometric measurements and electrochemical impedance spectra (EIS). Unless otherwise specified, experiments were performed by using 0.5 M H_2SO_4 as a supporting electrolyte. Before measurements, solutions were deaerated by bubbling ultrapure argon (99.9995%) for at least 20 min, and argon was continuously flowed over the surface of the electrolyte during measurements. The chrono amperometric measurements were carried out by, at first, holding the potential at E1 = 0 mV for 60 s, then setting to various potentials (E2) for 600 or 720 s. The amplitude of modulation potential for the EIS measurements was 10 mV, and the frequency was changed from 40 kHz to 50 mHz (for formic acid oxidation) or from 40 kHz to 20 mHz (for methanol oxidation). All experiments were performed at ambient temperature (22 ± 1 °C).

3 Results and discussion

3.1 Characterization of the nanoPtSn/Ti

The morphology of the nanoPtSn/Ti structure was studied using scanning electron microscopy (SEM). The SEM images of the nanoPtSn/Ti at different magnifications shown in Fig. 1a, b reveal the presence of nano-scale catalyst particles with the sizes of ca. 100–130 nm.

Figure 1b presents the nanoporous structure of the catalyst particles, showing the high stability of the catalyst. Energy Disperse Spectroscopy (EDS) of the nanoPtSn/Ti (Fig. 1c) shows the characteristic peaks of Pt at 1.5, 2.06 and 2.3 keV, and Sn at 3.44 and 3.7 keV. The atomic ratio of Pt to Sn in this sample is 27:6 according to the analysis of EDS. The XRD pattern of the catalyst shown in Fig. 1d presents the main characteristic peaks of the face-centered cubic (fcc) crystalline Pt at $2\theta = 39.4$, 45.5 and 67, namely, the planes (1 1 1), (2 0 0) and (2 2 0). The diffraction peaks appearing at $2\theta = 35.6$ and 62.8 can be attributed to the 101 and 112 indices of the tetragonal phase of β-Sn. No peaks for Sn oxides were found.

3.2 Cyclic voltammetric characteristics of nanoPtSn/Ti

To understand the electrochemical activity of the nanoPtSn/Ti, the cyclic voltammetric responses of the nanoPtSn/Ti and polycrystalline Pt electrodes were recorded in the potential range between −0.225 and 1.225 V at a scan rate of 50 mV s^{-1}. Figure 2 shows the CVs of the nanoPtSn/Ti and Pt in 0.5 M H_2SO_4 solution. Although the typical Pt-peaks for the hydrogen under-potential deposition (H_{udp}) and the oxidation of hydrogen (H_{oh}) are present on the nanoPtSn/Ti, they become ill-shaped compared to the pure Pt. The actual surface area of the nanoPtSn/Ti is equivalent to the number of Pt sites available for hydrogen adsorption/desorption. In calculating the adsorption charge, i.e. the integrated area under the peaks, we assume that the double layer capacitance is constant across the entire potential range. The hydrogen adsorption charge (Q_H) of polycrystalline Pt was calculated at 0.211 mC cm^{-2}. The nanoPtSn/Ti produced Q_H of 10.8 mC cm^{-2}. These results show that the real surface area of the sample is over 50 times higher than that of polycrystalline Pt. Furthermore, Fig. 2 shows that both oxidation and reduction current densities of CV on the nanoPtSn/Ti electrode are much higher than those on the polycrystalline Pt. For example, the reduction peak current density of oxides formed during the forward potential sweep on the nanoPtSn/Ti is 5.4 mA cm^{-2}, which is over 39 times higher than that on pure Pt. This indicates the presence of large numbers of active sites on the surface of nanoPtSn/Ti.

3.3 Formic acid oxidation

Figure 3 shows the cyclic voltammograms (CVs) of the nanoPtSn/Ti and pure Pt (the inset) in a 0.5 M HCOOH + 0.5 M H_2SO_4 solution. During the forward scan of the CV of pure Pt catalyst, the first anodic peak at 0.31 V results from formic acid oxidation, while the

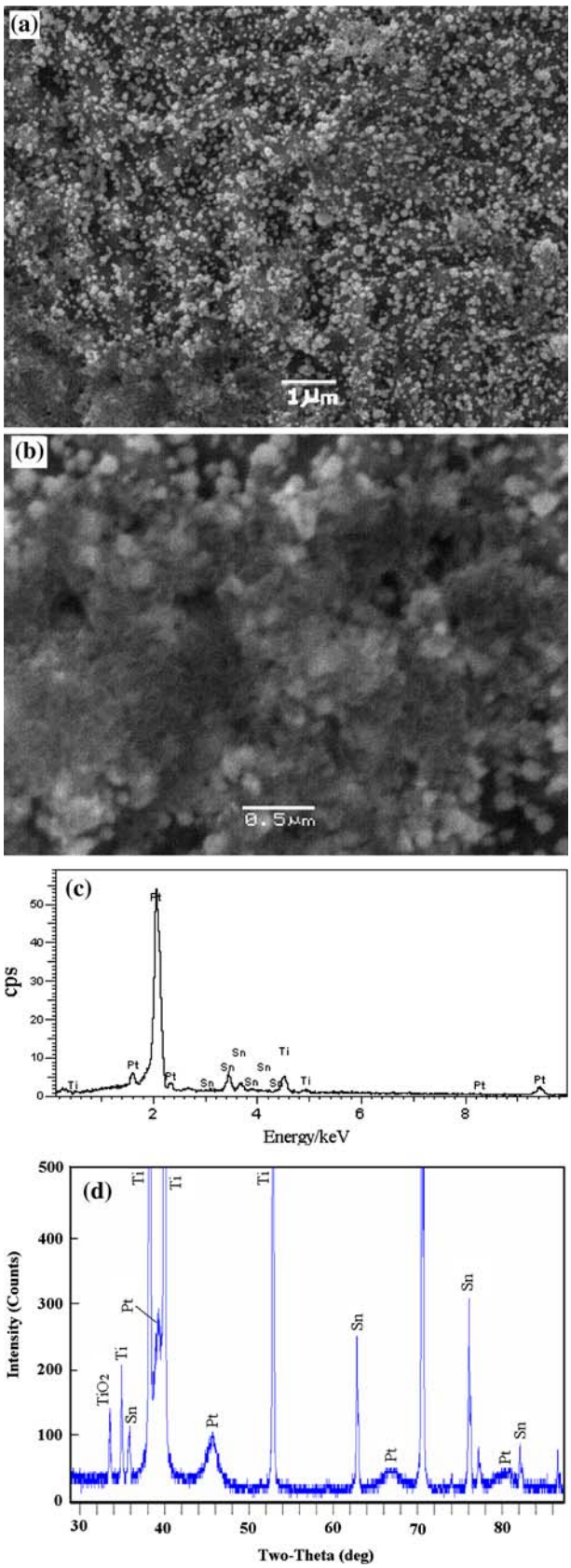

Fig. 1 Scanning electron micrographs (SEM) (**a**, **b**), energy disperse spectra (EDS) (**c**), and X-Ray Diffraction pattern (**d**) of nanoPtSn/Ti

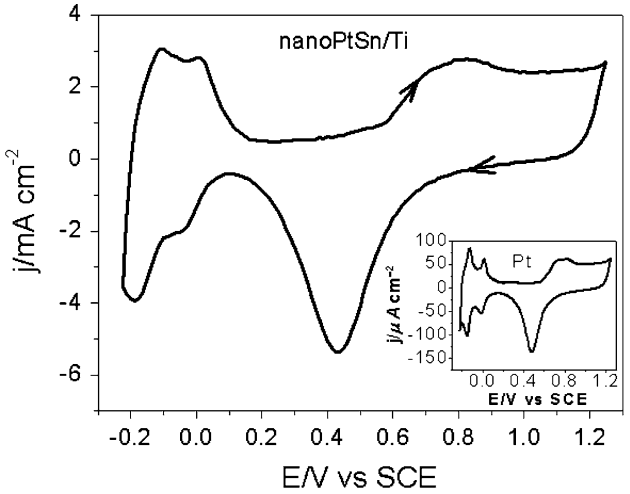

Fig. 2 Cyclic voltammograms of pure Pt (the inset) and nanoPtSn/Ti at the sweep rate of 50 mV s^{-1} in 0.5 M H_2SO_4

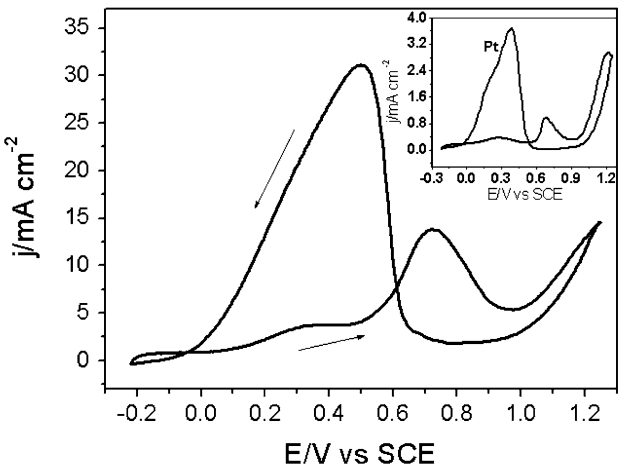

Fig. 3 Cyclic voltammograms of pure Pt (the inset) and nanoPtSn/Ti at the sweep rate of 50 mV s^{-1} in 0.5 M H_2SO_4 + 0.5 M HCOOH

second peak at 0.72 V can be attributed to CO oxidation and formic acid oxidation on sites that were previously blocked by CO [1]. The CV of nanoPtSn/Ti shows the usual characteristics of pure Pt except that both for forward and reverse scan directions the oxidation currents of formic acid on the nanoPtSn/Ti are significantly higher than on the Pt. It can be seen from voltammogram of HCOOH oxidation on the nanoPtSn/Ti that the reaction commences in the hydrogen region and proceeds slowly in the positive direction, and then reaches a plateau at ca. 0.3 V. At potentials more than ca. 0.45 V, the reaction becomes accelerated and a maximum rate at ca. 0.71 V occurs. A rapid increase in current density at potentials more than ca. 1.0 V is assigned to oxygen evolution. Upon reversing the potential sweep, a very steep increase of the reaction rate at ca. 0.75 V develops and a maximum current density is observed at ca. 0.5 V. After that, the current gradually

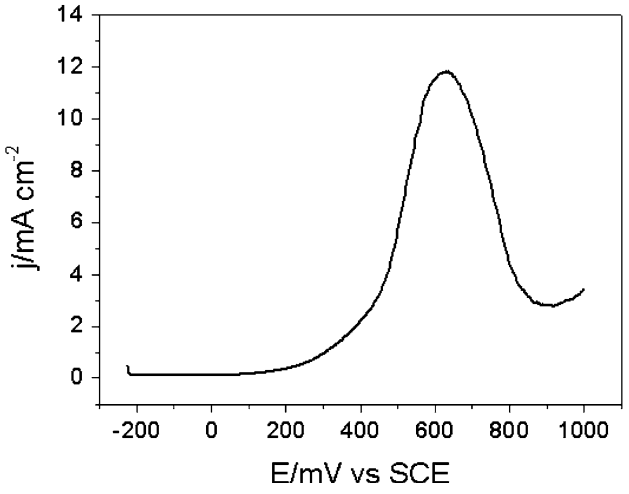

Fig. 4 Linear sweep voltammogram of nanoPtSn/Ti catalyst at the sweep rate of 1 mV s^{-1} in 0.5 M H_2SO_4 + 0.5 M HCOOH

decreases but the reaction rate is still faster than in the forward scan. This large anodic peak in the reverse scan is attributed to the removal of the incompletely oxidized carbonaceous species formed in the forward scan [29].

The pseudo steady state polarization curve of formic acid oxidation was also investigated at a slow potential scan rate of 1 mV s^{-1} (Fig. 4). It is observed that the oxidation rate shown in Fig. 4 remains almost the same as the forward scan of CV of Fig. 3. This further confirms that the formic acid oxidation is under activation control within the entire potential region [30, 31].

Chronoamperometric data of the nanoPtSn/Ti were recorded by potential steps from 0 mV for 60 s to the various potentials for 12 min. The current density-time transient for the HCOOH oxidation at different anodic potentials is shown in Fig. 5. The steady-state current density at $t = 720$ s increases with increase in applied potential. Phenomenologically, the oxidation current density increases slowly with time at 300 and 400 mV, while at higher potentials (500 and 600 mV) the current density increases sharply at short times and then decreases slowly at longer times. This may be caused by the CO-poisoning effect which results in deactivation of the catalyst surface and blocks further oxidation of formic acid.

In order to investigate the electrochemical reaction resistance of formic acid oxidation, electrochemical impedance spectroscopic measurements of the sample were carried out and analyzed. Nyquist plots of the nanoPtSn/Ti at various electrode potentials were recorded and are shown in Fig. 6. The frequency is changed from 40 kHz to 50 mHz. The impedances on both the imaginary and real axes are extremely low at the potentials shown in Fig. 6 except for 100 mV. This shows that the sample exhibits much lower charge transfer resistance and high electroactivity towards formic acid oxidation. The fitting equivalent

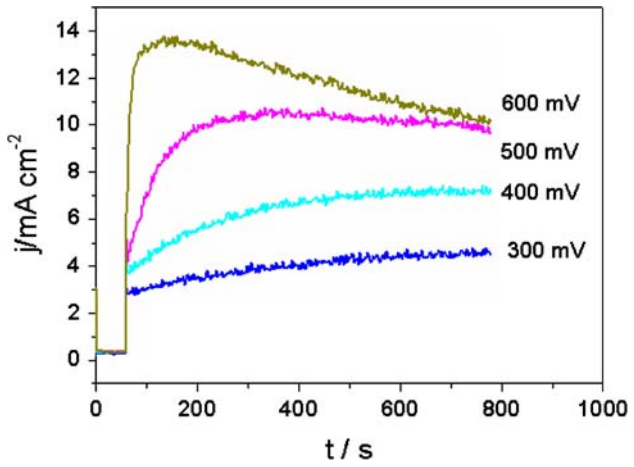

Fig. 5 Chronoamperometric data from nanoPtSn/Ti catalyst studied at different anodic potentials in 0.5 M H_2SO_4 + 0.5 M HCOOH. The potential was firstly held at E1 = 0 mV for 60 s, then set to E2 indicated in the plots

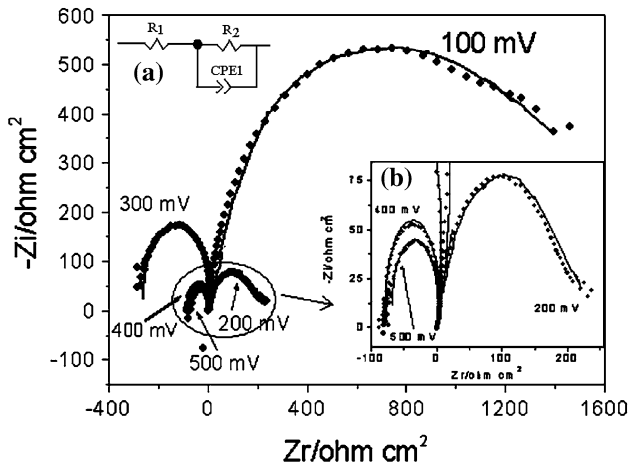

Fig. 6 Nyquist diagrams (dotted lines) of nanoPtSn/Ti catalyst at various potentials in 0.5 M H_2SO_4 + 0.5 M HCOOH and corresponding fitted curves (solid lines). Frequency was changed from 40 kHz to 50 mHz. Inset (a) is the corresponding equivalent electric circuit compatible with the Nyquist diagrams. Inset (b) shows the enlargement of elliptical selective region

circuit of the impedance spectra is shown in the inset (a) of Fig. 6, where R_1 represents the electrolyte resistance, R_2 is the charge transfer resistance and CPE shows the constant phase element. The corresponding data for each element are listed in Table 1. R_1 is in the range ca. 0.64–1.3 Ω cm^2 at different potentials due to the same supporting electrolyte (0.5 M H_2SO_4). R_2 (absolute value) decreases with potential except for 300 mV and becomes negative at 300, 400 and 500 mV. This is consistent with the negative real impedances at 300, 400 and 500 mV (Fig. 6). Another interesting observation from Fig. 6 is that the Nyquist diagrams deliver negative real impedances with decrease in frequency at potentials 300, 400 and 500 mV while

Table 1 Values of the elements in equivalent electric circuit fitted in the Nyquist plots of Fig. 6

Potential (mV)	R_1 (Ω cm^2)	R_2 (Ω cm^2)	CPE1-T	CPE1-P
100	0.95	1600	0.000374	0.75
200	0.84	230	0.000974	0.77
300	0.91	−255	0.000967	0.80
400	1.4	−77	0.00167	0.78
500	0.90	−68	0.0037	0.828

positive real impedance data occur at 100 and 200 mV. This is consistent with the similar electro-oxidation of methanol on the PtRu/C [32], e.g. electro-oxidation of formic acid on nanoPtSn/Ti could be simplified to two steps: one is adsorption of formic acid on the active sites of the catalyst to form adsorbed CO_{ads} followed by the further oxidation of the adsorbed species. At low potentials (100, 200 mV) adsorption of formic acid on the active sites of the PtSn/Ti surface may be the rate-determining step (r.d.s) for formic acid oxidation. This leads to an increase in charge-transfer resistance and presents positive impedances [32]. Conversely, the r.d.s. becomes the oxidation of the adsorbed species at higher potentials, leading to negative real impedance data [32], indicating the formation of a passivated catalyst [33].

3.4 Methanol oxidation

Electrochemical activity of the nanoPtSn/Ti towards methanol oxidation in 0.5 M H_2SO_4 was evaluated using cyclic voltammetric and chronoamperometric responses and EIS. Figure 7 shows the cyclic voltammograms (CV) of the sample and pure Pt (inset) in 0.5 M CH_3OH + 0.5 M H_2SO_4 at 50 mV s^{-1}. The CV profile of the nanoPtSn/Ti

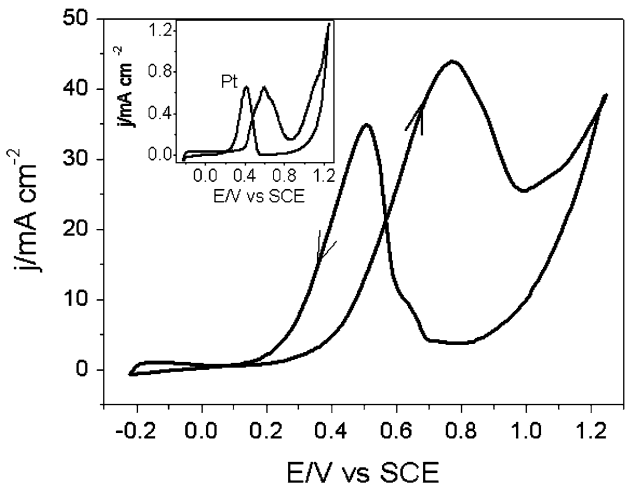

Fig. 7 Cyclic voltammograms of pure Pt (the inset) and nanoPtSn/Ti at the sweep rate of 50 mV s^{-1} in 0.5 M H_2SO_4 + 0.5 M CH_3OH

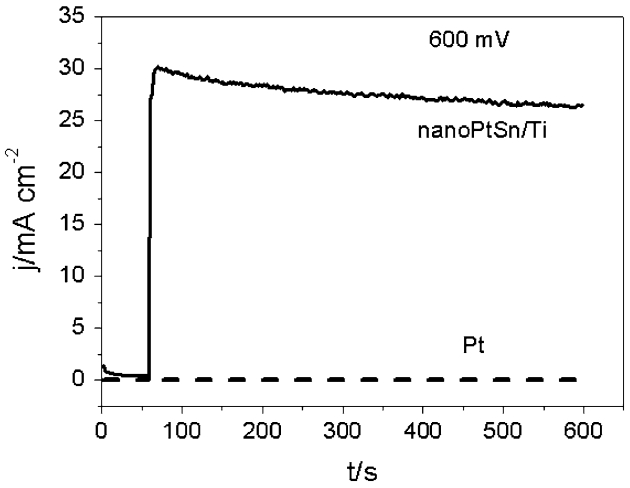

Fig. 8 Chronoamperometric data from nanoPtSn/Ti and Pt catalysts studied at 600 mV in 0.5 M H_2SO_4 + 0.5 M CH_3OH. The potential was firstly held at E1 = 0 mV for 60 s, then set to 600 mV

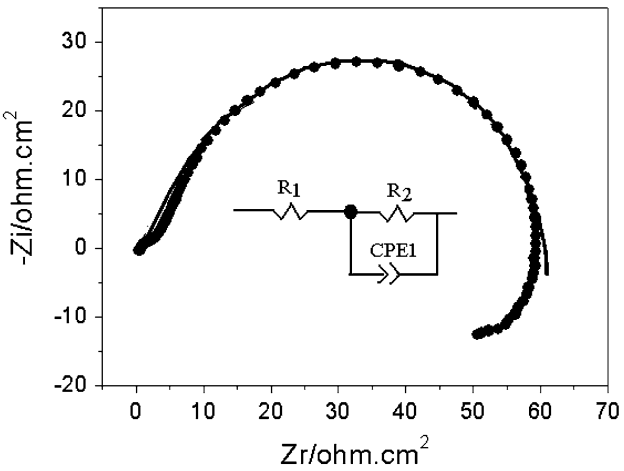

Fig. 9 Nyquist diagram (dotted line) of nanoPtSn/Ti catalyst at 300 mV in 0.5 M H_2SO_4 + 0.5 M CH_3OH and corresponding fitted curve (solid line). Frequency was changed from 40 kHz to 20 mHz. The inset is the corresponding equivalent electric circuit compatible with the Nyquist diagram

shows the usual characteristics of Pt except that the oxidation current densities on the nanoPtSn/Ti, both for the forward and backward scans, are much higher than on Pt, and moreover, they are higher than those on a similar Sn/Pt-bimetallic-nanotube electrode fabricated using a porous anodic aluminum oxide template [27]. In the scan towards positive potentials, the nanoPtSn/Ti electro-catalyst presents a methanol oxidation peak in the potential range 0.2–0.95 V. In the reverse scan, anodic currents are observed between 0.7 and 0.15 V. It is evident that nanoPtSn/Ti exhibits a lower onset potential of ca. 0.2 V and significantly higher current density for methanol oxidation than pure Pt. Consequently, nanoPtSn/Ti presents high methanol electro-oxidation activity, which may be directly related to the high electroactive surface areas of platinum nanoparticles [27].

The high electroactivity of nanoPtSn/Ti for methanol oxidation can be further observed from the chronoamperometric (CA) experiment. Figure 8 presents the CA data at 600 mV for the nanoPtSn/Ti and pure Pt in 0.5 M CH_3OH + 0.5 M H_2SO_4. A significant increase in steady-state current density for methanol oxidation on nanoPtSn/Ti occurs compared to pure Pt. The steady-state current densities of the nanoPtSn/Ti and pure Pt are 26.5 and 0.024 mA cm^{-2} (t = 600 s), respectively. This shows that the oxidation rate of methanol at 600 mV on nanoPtSn/Ti is about 1,000 times higher than that on Pt.

Figure 9 shows the Nyquist plot of the nanoPtSn/Ti in 0.5 M CH_3OH + 0.5 M H_2SO_4. The frequency was changed from 40 kHz to 20 mHz. The nanoPtSn/Ti has significantly low impedance, indicating that the nanoPtSn/Ti electrode shows low charge transfer resistances for methanol oxidation. The fitting equivalent circuit of the impedance spectroscopy is shown in Fig. 9 (inset). The corresponding fitted data for each element are listed in Table 2. The charge transfer resistance (R_2) is 60 Ω cm^2 at 300 mV in 0.5 M H_2SO_4 + 0.5 M CH_3OH, showing the high electroactivity of the nanoPtSn/Ti electrode for methanol oxidation.

Table 2 Values of the elements in equivalent electric circuit fitted in the Nyquist plot of Fig. 9

Potential (mV)	R_1 (Ω cm^2)	R_2 (Ω cm^2)	CPE1-T	CPE1-P
300	0.80	60.0	0.0009	0.870

4 Conclusions

I. Platinum and tin can be co-deposited on Ti using a simple hydrothermal process to form stable nano-size bimetallic particles.

II. Both in pure 0.5 M H_2SO_4 and 0.5 M HCOOH + 0.5 M H_2SO_4, the nanoPtSn/Ti presents similar cyclic voltammetric profiles to pure Pt. However, the nanoPtSn/Ti exhibits much high current density for formic acid oxidation. EIS shows that the nanoPtSn/Ti has very low charge transfer resistance. These results indicate that nanoPtSn/Ti exhibits high electroactivity for formic acid oxidation.

III. It was found from the cyclic voltammetric measurements in 0.5 M CH_3OH + 0.5 M H_2SO_4 that the electro-oxidation of CH_3OH on nanoPtSn/Ti commences at a lower anodic potential than on pure Pt. In addition, it was observed from the CVs and CAs that the nanoPtSn/Ti delivers much higher CH_3OH oxidation current densities than Pt.

IV. The high electrocatalytic activity of the nanoPtSn/Ti towards the oxidation of formic acid and methanol may be directly related to its large surface electroactive area.

Acknowledgements The authors thank A Project Supported by Scientific Research Fund of Hunan Provincial Education Department, China (07A019). Qingfeng Yi also thanks the Project Sponsored by the Scientific Research Foundation for Returned Overseas Chinese Scholars, State Education Ministry, China ([2007]1108).

References

1. Jayashree RS, Spendelow JS, Yeom J, Rastogi C, Shannon MA, Kenis PJA (2005) Electrochim Acta 50:4674
2. Golikand AN, Shahrokhian S, Asgari M, Maragheh MG, Irannejad L, Khanchi A (2005) J Power Sources 144:21
3. Khalil MW, Abdel Rahim MA, Zimmer A, Hassan Hanaa B, Abdel Hameed Randa M (2005) J Power Sources 144:35
4. Mancier V, Métrot A, Willmann P (1996) Electrochim Acta 41:1259
5. Abdel Rahim MA, Abdel Hameed RM, Khalil MW (2004) J Power Sources 134:160
6. Casella IG, Spera R (2005) J Electroanal Chem 578:55
7. Antolini E, Salgado Jose RC, Gonzalez ER (2006) Appl Catal B: Environ 63:137
8. Iwasita T, Xia XH, Herrero E (1996) Langmuir 12:4260
9. Aramata A, Kodera T, Masuda M (1988) J Appl Electrochem 18:577
10. Matare GJ, Tess ME, Yang Y, Abboud KA, McElwee-White L (2002) Organometallics 21:711
11. Gojkovic SLj, Vidakovic TR, Durovic DR (2003) Electrochim Acta 48:3607
12. Oliveira Neto A, Francoa EG, Arico E, Linardi M, Gonzalez ER (2003) J Eur Ceram Soc 23:2987
13. Solla-Gullon J, Vidal-Iglesias FJ, Montiel V, Aldaz A (2004) Electrochim Acta 49:5079
14. Kim C, Jung Kim Y, Am Kim Y, Yanagisawa T, Chul Park K, Endo M, Dresselhaus MS (2004) J Appl Phys 96:5903
15. Liu Z, Yang Lee J, Chen W, Han M, Ming Gan L (2004) Langmuir 20:181
16. Spinacé EV, Neto AO, Linardi M (2004) J Power Sources 129:121
17. Yang Y, McElwee-White L (2004) Dalton Trans 15:2352
18. Rojas S, García-Garcı FJ, Järas S, Martínez-Huerta MV, Luis García Fierro J, Boutonnet M (2005) Appl Catal A: Gen 285:24
19. Yi Q, Chen A, Huang W, Zhang J, Liu X, Xu G, Zhou Z (2007) Electrochem Commun 9:1513
20. Liao S, Holmes K-A, Tsaprailis H, Birss VI (2006) J Am Chem Soc 128(11):3504
21. Ha S, Larsen R, Msel RI (2005) J Power Source 144:28
22. Li X, Hsing I-M (2006) Electrochim Acta 51:3477
23. Stalnionis G, Tamasauskaite-Tamasiunaite L, Pautieniene V, Jusys Z (2004) J Solid State Electrochem 8:900
24. Golikand AN, Golabi SM, Maragheh MG, Irannejad L (2005) J Power Sources 145:116
25. Leger J-M (2005) Electrochim Acta 50:3123
26. Jiang L, Sun G, Sun S, Liu J, Tang S, Li H, Zhou B, Xin Q (2005) Electrochim Acta 50:5384
27. Guo YG, Hu JS, Zhang HM, Liang HP, Wan LJ, Bai CL (2005) Adv Mater 17:746
28. Liu Z, Guo B, Hong L, Han Lim T (2006) Electrochem Commun 8:83
29. Zhang L, Wang Z, Xia D (2006) J Alloys Compd 426:268
30. Lovic JD, Tripkovic AV, Gojkovic SLj, Popovic KDj, Tripkovic DV, Olszewski P, Kowal A (2005) J Electroanal Chem 581:294
31. Jiang J, Kucernak A (2002) J Electroanal Chem 520:64
32. Wu G, Li L, Xu B (2005) Chem J Chin Univ 26:715
33. Melnick RE, Palmore GTR (2001) J Phys Chem B 105:1012, 9449